UTAH VALLEY UVU UNIVERSITY Department of EARTH SCIENCE

Applications of Structure from Motion Software in Earthquake Geology Investigations: Examples from the Wasatch, Oquirrh, and San Andreas Faults

Michael Bunds (michael.bunds@uvu.edu), Nathan Toké, Suzanne Walther, Andrew Fletcher, and Michael Arnoff, Department of Earth Science, Utah Valley University

UTAH VALLEY UVU UNIVERSITY Department of EARTH SCIENCE

Introduction

Structure from Motion (SfM) is a photogrammetry method that enables construction of accurately georeferenced and scaled point clouds of the surfaces of objects from multiple photographs for which there is little or no apriori information on camera position, orientation, or lens characteristics. Insofar as it produces point clouds of surfaces, the resulting data sets are similar in many ways to those produced by terrestrial and airborne LiDAR (TLS and ALS, respectively).

We show SfM methods applied to trench logging, as well as equipment, methods, and results for the rapidly emerging SfM application of generating high accuracy and ultra-high resolution DEMs and orthophotos from aerial imagery acquired with a UAV and processed with commercially available Agisoft Photoscan software.

Comparison of SfM to LiDAR

SfM Advantages

- Low Cost
- Rapid deployment
- High spatial resolution relative to airborne LiDAR (ALS)
- Orthophoto can be easily produced

SfM Disadvantages

- Potentially less accurate than ALS, significantly less accurate that terrestrial LiDAR (TLS)
- Difficult or impossible to strip vegetation
- Time – consuming to cover a large area (1 to a few km^2 per day possible)
- Legal and ethical issues flying UAV in developed areas

Methods

Equipment

UAV: DJI Phantom II quadcopter (inexpensive, hobbyist-grade)
Camera: GoPro Hero 3 Black Edition
GNSS Survey equipment: Trimble R8 and/or Trimble 5700
Software: Agisoft Photoscan (v 1.0.4 to date)
Computers: A range of machines from an i7 laptop to 6-core i7 PCs with 32GB RAM and NVIDIA GTX 970 GPUs; high performance machines reduce processing times by 10 to 20 times vs our standard i7 desktop computers

Workflow to Build DEM from UAV-derived Aerial Imagery

1. Place and measure control points
2. Acquire aerial imagery
3. Select images to be used in model
4. Correct lens distortion
5. Align Photos ("Structure from Motion")
6. Incorporate control point locations in model and adjust camera models
7. Build dense point cloud ("Multi-view Stereo")
8. Convert point cloud to gridded DEM

Above: Trimble R8 survey-grade GNSS rover set-up on a ground control point along the San Andreas fault near Dry Lake Valley, California. We use the R8 in VRS, RTK, and fast-static mode, depending on the situation, to obtain control point locations with 1 to 2 cm 2-sigma accuracy.

Above: DJI Phantom II quadcopter, GoPro Hero 3 Black Edition camera, and Zenmuse H3-3D gimbal used for acquisition of aerial photographs. The UAV is equipped with a WiFi system that relays video from the GoPro to a ground-based monitor in real time to aid navigation and positioning of the UAV during flights.

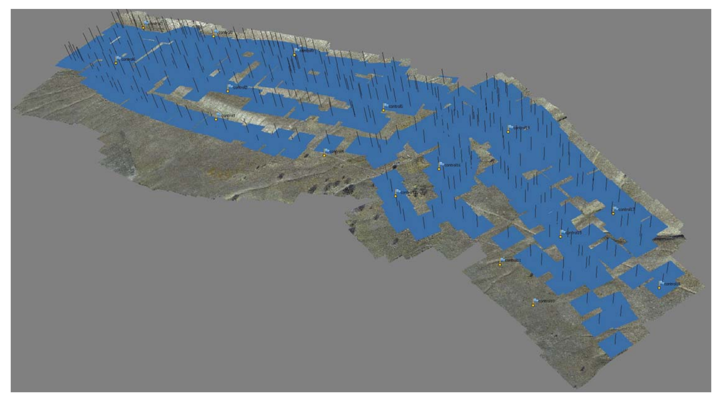

Point cloud of Flood Canyon area with camera locations and orientations shown by blue rectangles and orthogonal black lines. Screenshot from Agisoft Photoscan.

References

Bemis, S., Micklethwaite, Turner, James, Aksciz, Thiele, Bangash, 2014, Ground-based and UAV-based photogrammetry: A multi-scale, high-resolution mapping tool for structural geology and paleoseismology, J. Struct. Geol., v69, 163-178, *http://www.sciencedirect.com/science/article/pii/S0191814114002429*
Heidemann, H.K., 2014, Lidar base specification, (v 1.2, November 2014): USGS Techniques and Methods, book 11, ch. B4, 67 pp, *http://dx.doi.org/10.3133/tm1184*
James, M.R., Robson, S., 2012, Straightforward reconstruction of 3D surfaces and topograpy with a camera: accuracy and geoscience application, JGR v117, F03017, *http://dx.doi.org/10.1029/2011JF002289*
James, M.R., Robson, S., 2014, Mitigating systematic error in topographic models derived from UAV and ground-based image networks, Earth Surf. Proc. & Landforms, v39, 1413-1420, *http://dx.doi.org/10.1002/esp.3609*
Johnson, K., E. Nissen, S. Saripalli, J.R. Arrowsmith, P. McGarey, K. Scharer, P. Williams, K. Blisniuk, 2014, Rapid mapping of ultrafine fault zone topography with structure from motion, Geosphere, *http://dx.doi.org/10.1130/GES01017.1*
Toké, N. A., J.B. Salisbury, J.R. Arrowsmith, L.T. Kellum, E. Matheson, J.K. Carlson, D. Horns, T. Sato, N. Abueg, J. Anderson, and J. Selck, 2013, Documenting at least 1300 years of aseismic slip: enechelon shear bands and small-scale ground cracking at the Dry Lake Valley Paleoseismic site along the central San Andreas Fault, Annual Southern California Earthquake Center Meeting, Proceedings and Abstracts v23.
Toké, N., M. Arnoff, J. Thomas, and M. Bunds, 2015, Documenting recent rupture traces and opportunistic paleoseismic exposures from the northern Provo Segment to the southern Salt Lake City Segment of the Wasatch Fault, Basin and Range Seismic Hazard Summit III, Salt Lake City, UT.
Watershed Sciences, 2014, State of Utah LiDAR 2013/2014 Technical Data / Project History Report, *ftp://ftp.agrc.utah.gov/Imagery/LIDAR/WasatchFront_2013_2014/WasatchFront_2013_2014_LiDAR_Report.zip*

San Andreas Fault at Dry Lake Valley, California

To capture small-scale creep-induced fracture sets in soil on the San Andreas Fault, we used two sets of photographs, one consisting of 62 photos, the other 55, taken at different heights to produce DEMs at two different scales. Only 4 control points were measured, so the long wavelength elevation accuracy of the DEMs is limited, but their high resolution allows good imaging of the fracture sets. The area is vegetated with grass and isolated trees, which makes it well suited to constructing a DEM from aerial imagery.

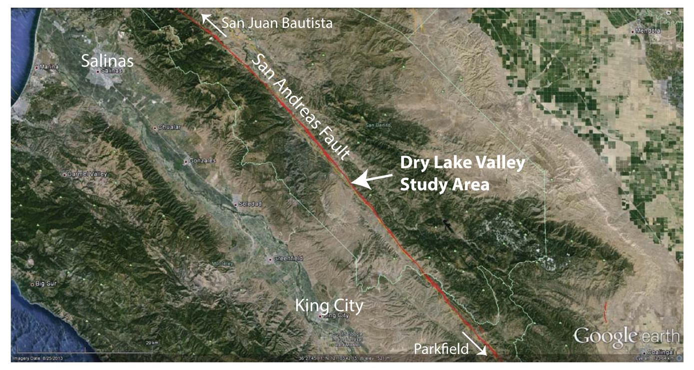

Location of Dry Lake Valley study area on the creeping segment of the San Andreas Fault, central California. Google Earth imagery, faults from the USGS Quaternary fault and fold datase (U.S. Geological Survey and California Geological Survey, 2006, Quaternary fault and fold database for the United States, accessed 1/10/2015, *http://earthquakes.usgs.gov-/regional/qfaults)*

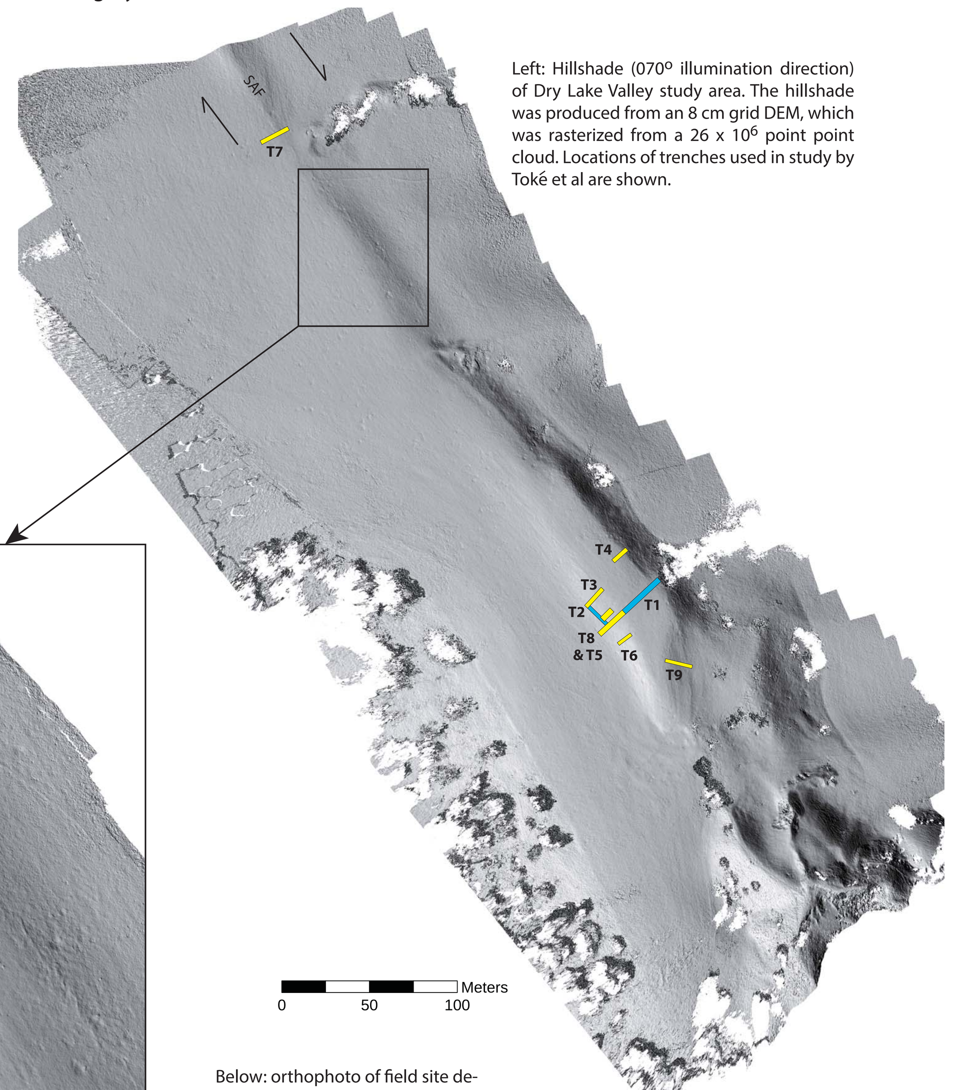

Left: Hillshade (070º illumination direction) of Dry Lake Valley study area. The hillshade was produced from an 8 cm grid DEM, which was rasterized from a 26 x 10^6 point point cloud. Locations of trenches used in study by Toké et al are shown.

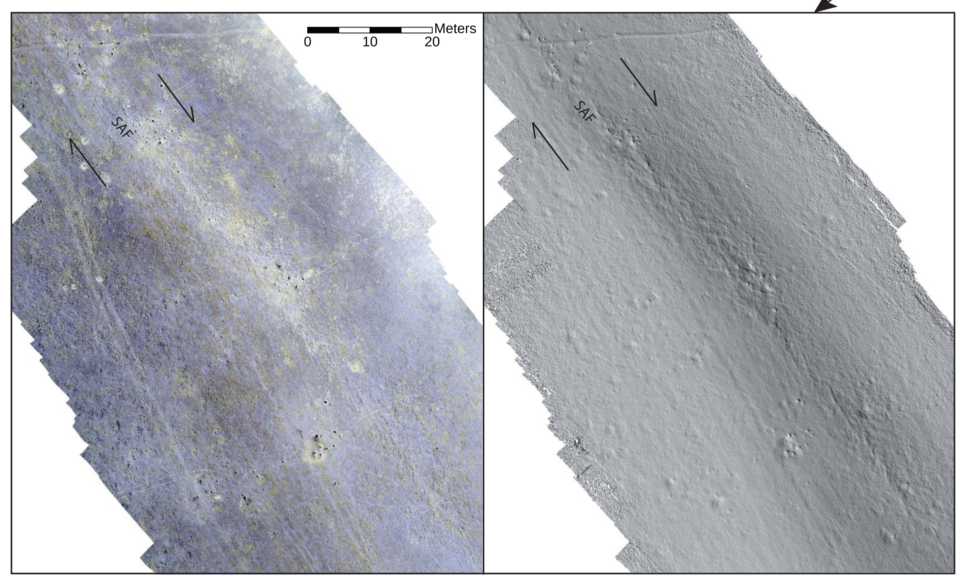

Detail imagery from SfM of fractures along fault trace. Orthophoto on left, hillshade (070º illumination direction) on right. The hillshade was made from a 3 cm grid DEM.

Below: orthophoto of field site derived from the same point cloud as hillshade above. 1 cm pixel size.

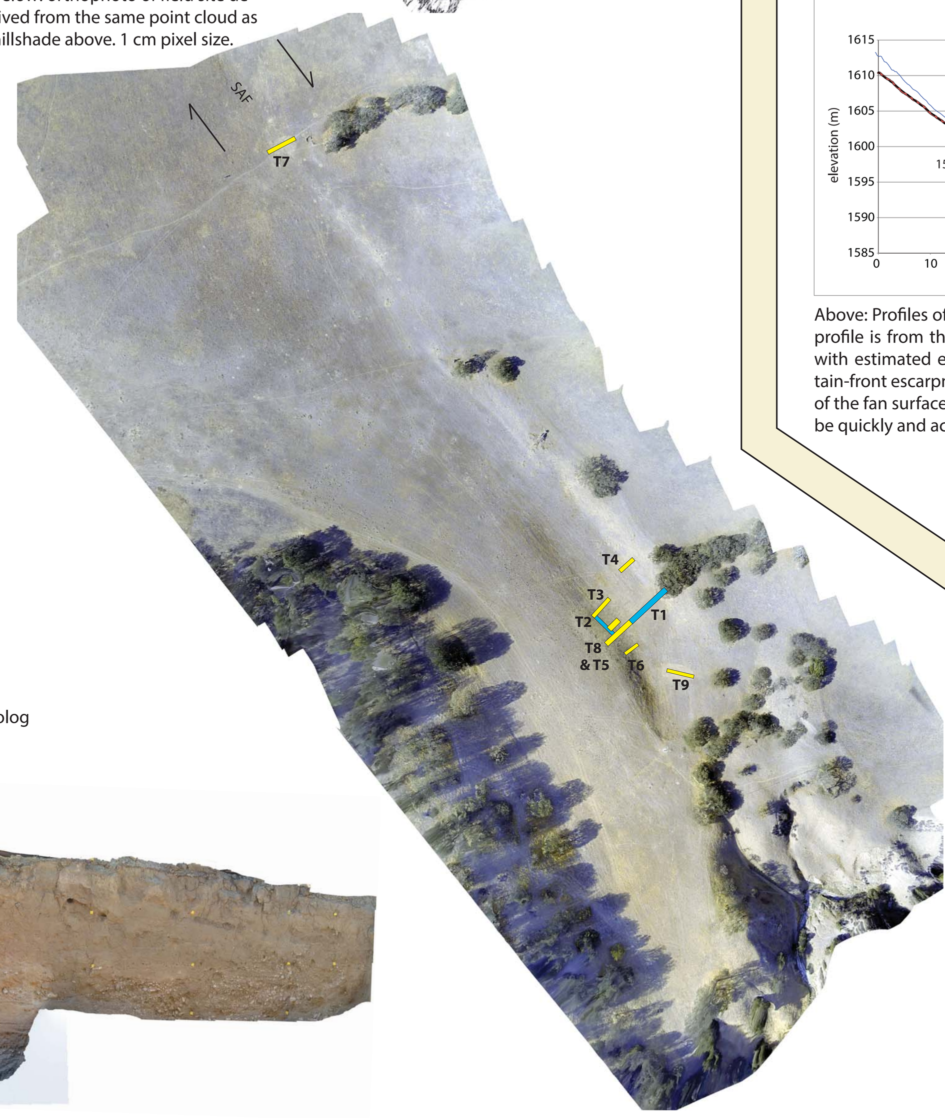

Left: Trench 7 southeast wall photolog generated using SfM; oblique view. Photolog is a scaled 3-d model that can be rotated during viewing on a computer.

Above: Trench 8 southeast wall photolog generated using SfM; oblique view. Photolog is a scaled 3-d model that can be rotated during viewing on a computer.

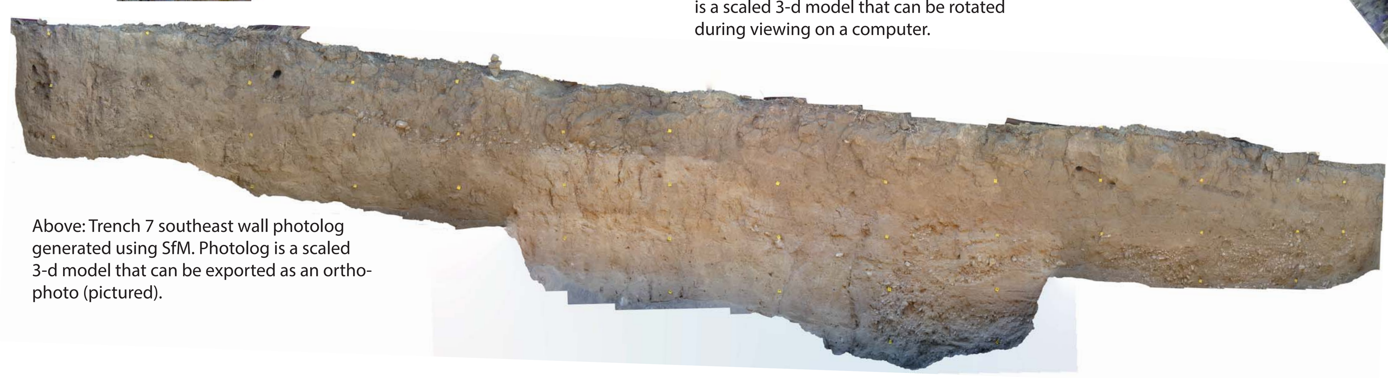

Above: Trench 7 southeast wall photolog generated using SfM. Photolog is a scaled 3-d model that can be exported as an orthophoto (pictured).

Oquirrh Fault at Flood Canyon, Tooele County, Utah

The Oquirrh fault is a west-dipping normal fault along the west side of the Oquirrh Mountains. We produced a DEM of an area that spans the fault and a series of Lake Bonneville benches near Flood Canyon, in an effort to accurately estimate post-Bonneville cumulative displacement on the fault. The DEM covers ~ 1 km^2, has a 12 cm grid spacing, is derived from a 150 x 10^6 point point cloud made from 335 photos, and the RMS error in elevation is 15 cm. One field day and one day of processing were required to produce the DEM. Vegetation is limited to grass and weeds less than 1 m tall.

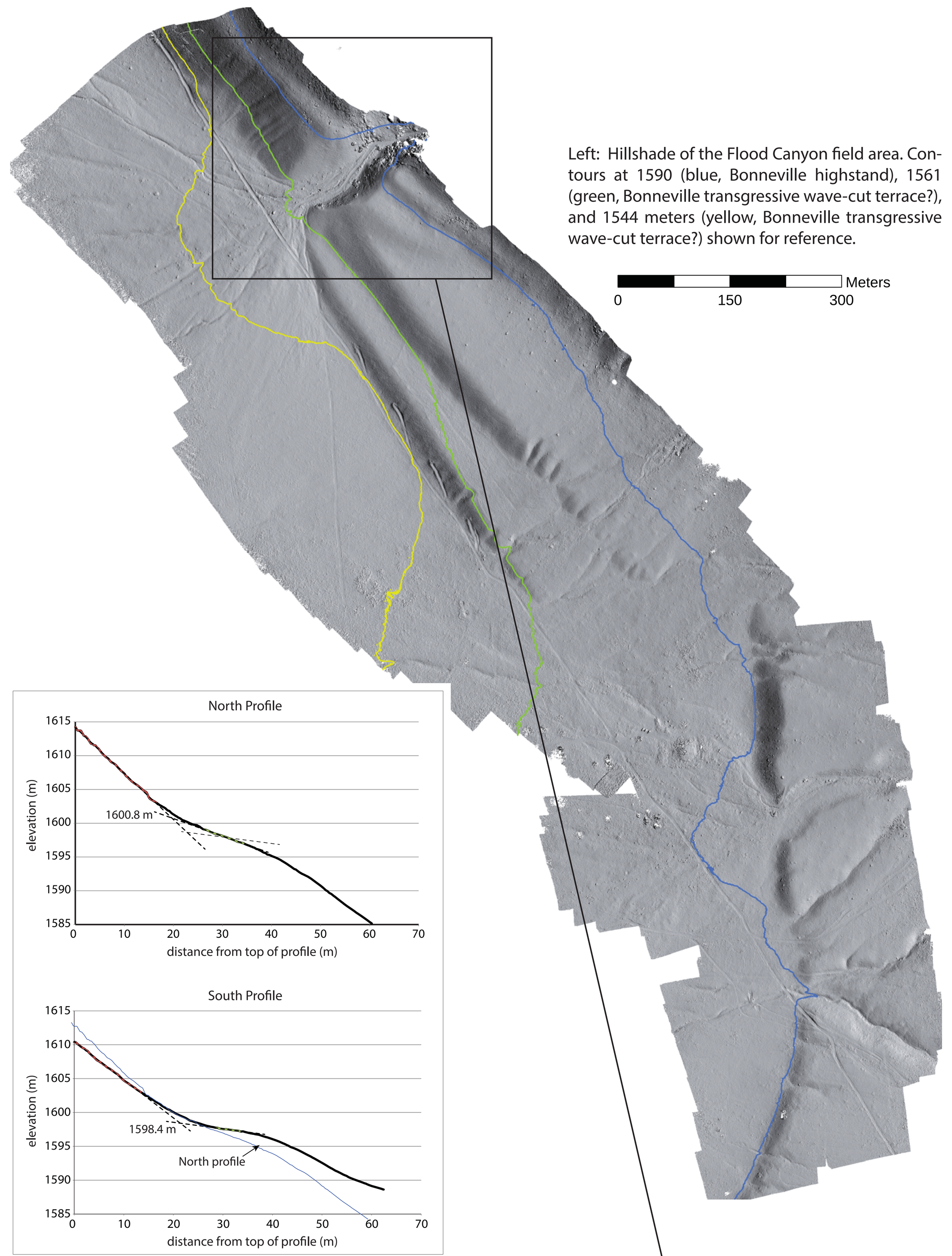

Left: Hillshade of the Flood Canyon field area. Contours at 1590 (blue, Bonneville highstand), 1561 (green, Bonneville transgressive wave-cut terrace?), and 1544 meters (yellow, Bonneville transgressive wave-cut terrace?) shown for reference.

Above: Profiles of a fan surface that spans the Oquirrh fault (the north profile is from the footwall, the south profile from the hanging wall) with estimated elevations of intersections of fan surface and mountain-front escarpment. Offset across the fault is uncertain (as is the age of the fan surface), but the profiles exemplify the type of data that can be quickly and accurately extracted from DEMs derived from SfM.

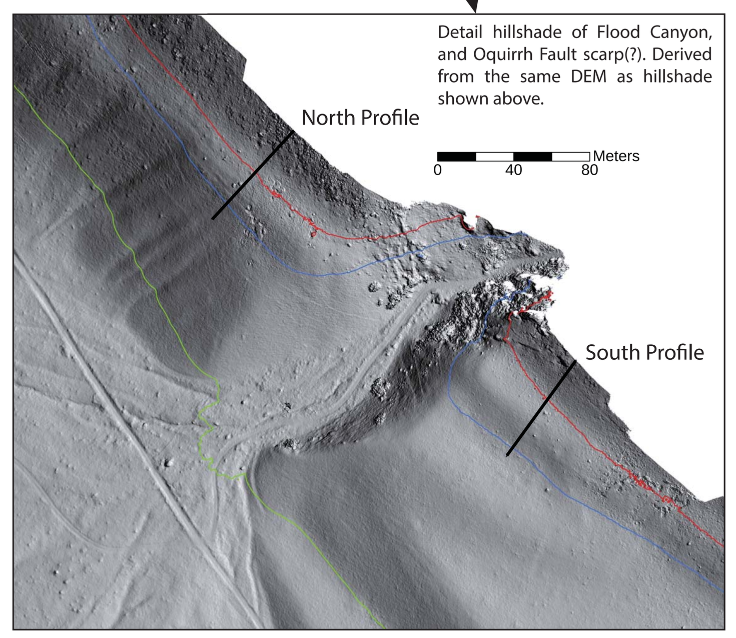

Detail hillshade of Flood Canyon, and Oquirrh Fault scarp(?). Derived from the same DEM as hillshade shown above.

Oquirrh and Wasatch Fault Location Map

Location map for Flood Canyon (Oquirrh Fault) and Box Elder Canyon (Wasatch Fault) study areas. Google Earth imagery, faults from the USGS Quaternary fault and fold datase (U.S. Geological Survey and Utah Geological Survey, 2006, Quaternary fault and fold database for the United States, accessed 1/10/2015, *http://earthquakes.usgs.gov/regional/qfaults)*

Wasatch Fault at Box Elder Canyon, Utah County, Utah

A DEM of a small section of the Wasatch Fault was produced for three reasons: 1) to test use of a high-resolution DEM for fault scarp mapping needed for relocation of the pictured water tank, 2) to aid paleoseismology work in an adjacent arroyo, and 3) for comparison with new 0.5 m airborne LiDAR of the Wasatch Front in an area challenging to SfM due to moderate vegetation coverage. Two point clouds, with 10×10^6 and 118×10^6 points respectively, were made from 149 photos. 6 and 20 cm grid DEMs were rasterized from the point clouds. The DEMs have 10 cm RMS error. The SfM DEM captures bare earth morphology similarly to the LiDAR. The lower density SfM point cloud and DEM is in some ways superior to the higher resolution SfM DEM for interpreting bare Earth topography, but the high density point cloud and DEM offers markedly better resolution than the ALS.

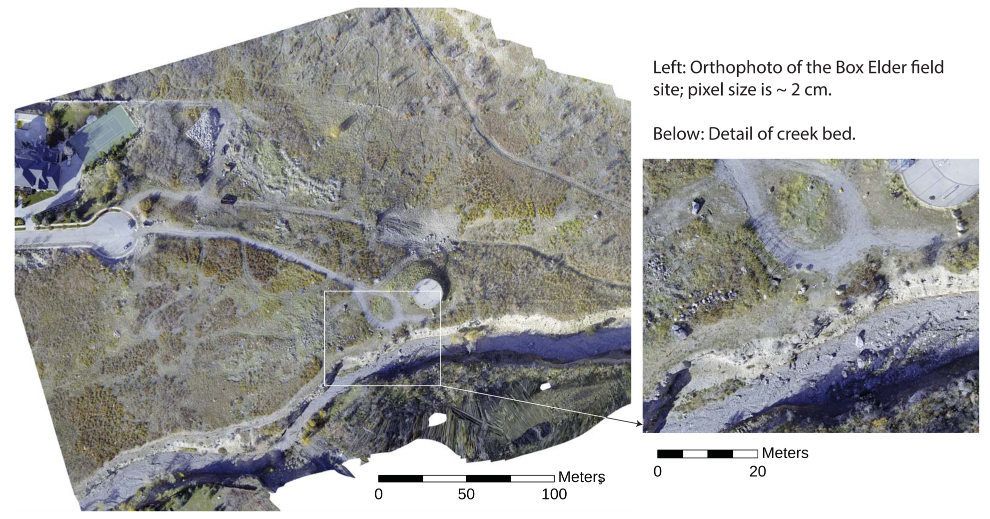

Left: Orthophoto of the Box Elder field site; pixel size is ~ 2 cm.

Below: Detail of creek bed.

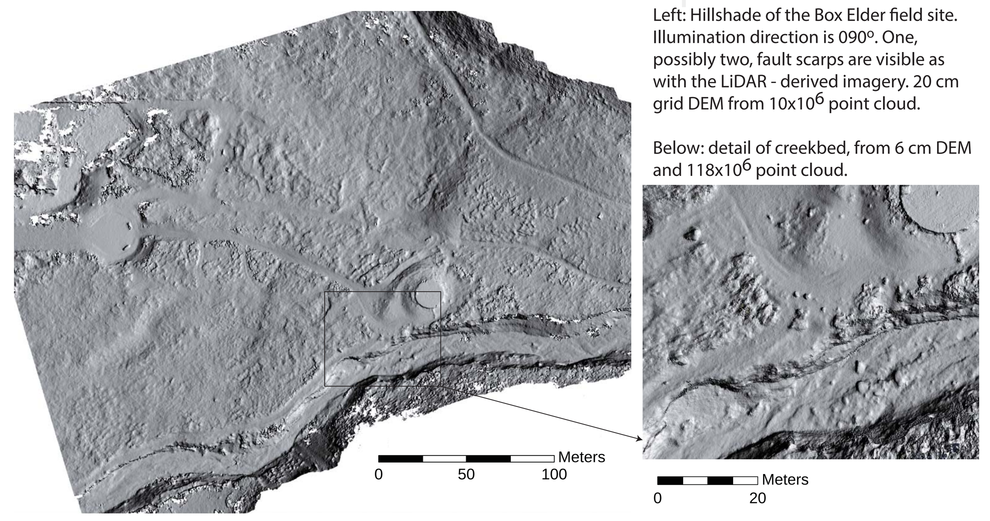

Left: Hillshade of the Box Elder field site. Illumination direction is 090º. One, possibly two, fault scarps are visible as with the LiDAR - derived imagery. 20 cm grid DEM from 10×10^6 point cloud.

Below: detail of creekbed, from 6 cm DEM and 118×10^6 point cloud.

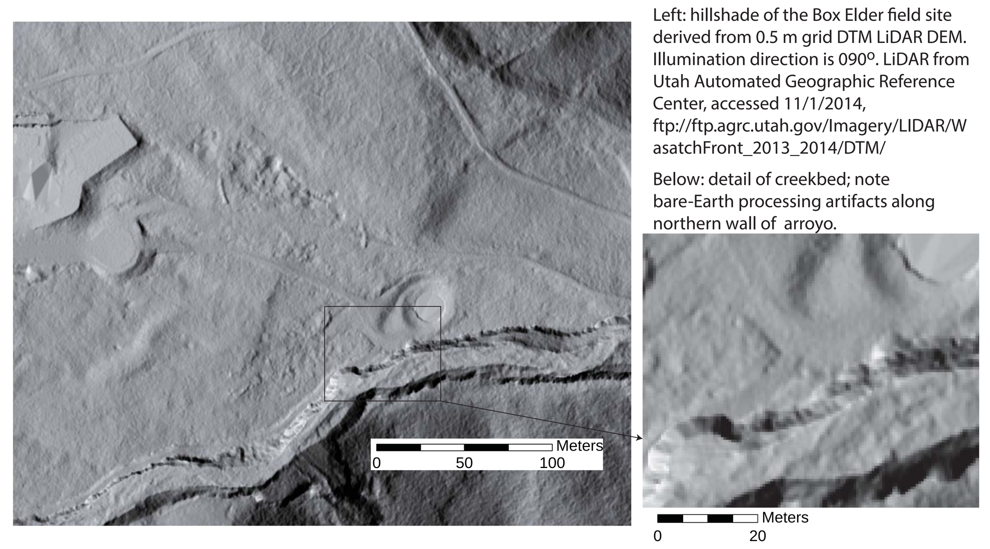

Left: hillshade of the Box Elder field site derived from 0.5 m grid DTM LiDAR DEM. Illumination direction is 090º. LiDAR from Utah Automated Geographic Reference Center, accessed 11/1/2014, ftp://ftp.agrc.utah.gov/Imagery/LIDAR/WasatchFront_2013_2014/DTM/

Below: detail of creekbed; note bare-Earth processing artifacts along northern wall of arroyo.